Departmental Papers (MSE)   Department of Materials Science & Engineering

7-1-2003

Effect of Seeding on the Microstructure and Mechanical Properties of alpha-SiAlON: III, Comparison of Modifying Cations

Misha Zenotchkine
University of Pennsylvania

Roman Shuba
University of Pennsylvania, rshuba@seas.upenn.edu

I-Wei Chen
University of Pennsylvania, iweichen@seas.upenn.edu

journal

Effect of Seeding on the Microstructure and Mechanical Properties of α-SiAlON: III, Comparison of Modifying Cations

M. Zenotchkine, R. Shuba, and I-Wei Chen*

Department of Materials Science and Engineering, University of Pennsylvania,
Philadelphia, Pennsylvania   19104-6272

Single-phase *in situ* toughened SiAlON ceramics containing various modifying cations and single-crystal seeds were studied. The modifying cations include rare-earth cations from the smallest to the largest allowed in the α-SiAlON structure (Yb to Y, to Nd), and from monovalent to trivalent (Li to Ca, to rare earths). At low seeding levels, the aspect ratio of grains increases with the size of modifying cations, giving rise to rather different appearances of the microstructure in different SiAlONs. A one-to-one correspondence between seed crystals and large grains at low seeding levels is also observed. An optimal amount of seeds is required to maximize the fracture toughness, which is controlled by grain pullout with the fracture energy that scales with the fraction of elongated grains, their width, and their aspect ratio. The optimal amount of seeds required to reach maximal toughening increases with the aspect ratio of grains and is the lowest (1%) in Y- and Yb-SiAlONs.

I.   Introduction

SEEDING is a well-established method for controlling phase nucleation and growth in ceramics. For α-SiAlON, this approach has been investigated in detail using Y-SiAlON[1–3] and Ca-SiAlON[2,4] as model systems. In both cases, seeds were expressly grown as small single crystals and had compositions matching those of the ceramics.[5,6] These seeds are highly effective in producing large elongated grains. In particular, when the amount of seeds is small, an essentially one-to-one correspondence between seeds and the large elongated grains has been observed. As the amount of seeds increases, the large elongated grains that they produce begin to impinge with each other, so the microstructure eventually refines again. Maximum toughness is therefore associated with an intermediate seed content, which varies from about 1% in Y-SiAlON[3] to about 4%–8% in Ca-SiAlON.[4] It has also been found that, unlike unseeded α-SiAlONs in which the nucleation and growth of large grains are extremely sensitive to the heating schedule, seeded α-SiAlONs usually have relatively similar microstructures over a broad range of processing conditions.[7] Therefore, with single-crystal seeds, a definitive control of the microstructure and mechanical properties of α-SiAlON becomes feasible.

Phase relations of α-SiAlONs, however, vary significantly from system to system depending on the interstitial cations that they contain.[8] Therefore, to generalize our findings to other α-SiAlONs, we have investigated three additional systems that contain Li, Nd, and Yb, respectively. Together with our previous work,[3,4] hereafter referred to as Parts I and II, the study covers α-SiAlONs with interstitial rare-earth cations from the smallest to the largest allowed (Yb, Y, to Nd), and from monovalent to trivalent (Li, Ca, to rare earths.) As will become clear in the following, we were also able to directly view seed crystals on the polished cross sections of some SiAlONs, thereby to definitely identify grains that derived from the seeds. This allows us to obtain a detailed understanding of seeding statistics, and to systematically compare grain growth in different α-SiAlONs. A further attempt to correlate the toughness to grain parameters has also been made to clarify the origin of fracture resistance and its relation to optimal microstructure.[3,4]

II.   Experimental Procedure

(1)   Compositions

The compositions investigated in our experiments lie near the center of the single-phase region of α-SiAlON represented by the formula $M_{m/z}Si_{12-(m+n)}Al_{m+n}O_nN_{16-n}$. Here M is an interstitial cation that has a valence *z*. Specifically, they are the following: M = Yb, *m* = 1.5, and *n* = 1.2 (Yb1512); M = Nd, *m* = 1.3, and *n* = 1.1 (Nd1311); M = Y, *m* = 1.5, and *n* = 1.2 (Y1512); M = Ca, *m* = 1.5, and *n* = 1.2 (Ca1512); and M = Li, *m* = 1.5, and *n* = 1.2 (Li1512). A smaller *m* is used for Nd1311 because of the smaller single-phase region of α-SiAlON in this system. The data of Y1512 and Ca1512 have been reported in our previous publications.

(2)   Seed Crystals

Seed crystals of Yb-, Nd-, Y-, Ca-, and Li-α-SiAlON with compositions matching the above α-SiAlON were obtained from a liquid-growth process described elsewhere.[5,6] Briefly, powder mixtures of appropriate compositions were fired in a gas pressure sintering furnace at various temperatures: 1650°C for Yb-α-SiAlON seeds, 1700°C for Y-, Ca-, and Li-α-SiAlON seeds, and 1850°C for Nd-α-SiAlON seeds. The holding time was 2 h and the atmosphere was nitrogen at 10 MPa. The fired compacts were milled and subsequently washed in acids to remove the residual phases. The seed crystals harvested were found by X-ray diffraction (XRD) to consist of single-phase α-SiAlON, with lattice parameters that are essentially the same as those α-SiAlON ceramics of the above-mentioned compositions. The dimensions of seed crystals were analyzed for more than 200 crystals per sample using micrographs obtained by a scanning electron microscopy (SEM). With the exception of Li1512 composition, which gave equiaxed crystals, elongated seeds with geometry of a hexagonal rod were observed. The average width (*W*) and length (*L*) of these seeds are listed in Table I.

(3)   Powder and Ceramic Processing

Starting powder mixtures were prepared from α-Si₃N₄ (SN-E10, Ube Ind., Ube, Japan), AlN (type F, Tokuyama Soda Co., CA), Al₂O₃ (AKP50, Sumitomo Chemical America, NY), Yb₂O₃/Nd₂O₃/Y₂O₃ (99.9%, ALFA-Johnson Matthew Co., MA), CaCO₃

Table I. Average Width (*W*) and Length (*L*) of Seed Crystals of Different Compositions

	Modifying cation				
Seed dimensions	Y	Yb	Nd	Ca	Li
W (μm)	0.71 ± 0.19	0.61 ± 0.16	0.92 ± 0.51	0.33 ± 0.10	2.12 ± 1.28
L (μm)	1.71 ± 0.63	1.28 ± 0.41	3.96 ± 0.51	0.86 ± 0.28	2.33 ± 1.34

(CS-3NA, Pred Materials, Inc., NY), and Li_2CO_3 (99+%, Aldrich Chemical Co., WI). The oxygen content in α-Si_3N_4 (1.24 wt%) and AlN (0.88 wt%) was taken into account in the formulation. Methods for powder and ceramic processing were the same as described in our previous papers.[1–4] Briefly, powder mixtures (including seeds) were attrition-milled in isopropyl alcohol and subsequently dried under a halogen lamp. Charges of 20 g of powders were hot-pressed, under 30 MPa, in a graphite resistance furnace at 1900°C for 1 h in a nitrogen atmosphere. The heating rate used to reach the above temperature was 20°C/min. Full densification was achieved in all experiments. The phase purity and the chemical composition of the pulverized ceramics were examined using XRD. In all cases, only single-phase α-SiAlON reflections were observed, with corresponding lattice parameters very similar to those of the published data for the intended compositions.[9–11]

(4) Ceramic Characterization

Microstructures of ceramic samples were observed on polished sections after etching. The etchants used were a boiling solution of 20 g of NH_4F in 50 mL of HNO_3 for Yb-, Nd-, and Y-SiAlON,[12] and molten KOH for Ca- and Li-SiAlON. SEM micrographs were used for microstructure characterization. *R*-curves were measured in four-point bending using bars with dimensions of 30 mm × 4 mm × 2 mm, with their tensile surfaces lying parallel to the hot-pressing planes. These bars contained initial notches ~0.1–0.2 mm deep with a tip radius of 10 μm. Crack length was measured *in situ* under a microscope that had a resolution of 2–5 μm. Further details of the above procedures are available elsewhere.[2–4,7] In the case of Li1512, no stable crack extension was observed in our experiment. Therefore, only a single fracture toughness value

obtained with the single-edge-notched beam (SENB) of the above geometry is reported.

Grain statistics were investigated by first tracing the contours of grain boundaries on SEM micrographs, then using the "Clemex Vision" software (Clemex Technologies, Inc.) to analyze the dimensions and surface area of 1000–3000 grains per sample. In the case of Y1512 and Yb1512, our etching method readily revealed a core–shell microstructure for those grains with the seed crystals exposed as the cores. This is because the interface between the seed and the outer grain was more severely etched. Therefore, the statistics of those grains with a discernible core are also analyzed for these compositions.

III. Results and Analysis

(1) Grain Shape

A most important difference between different seeded SiAlONs is the shape of large grains produced by seeds. This is best illustrated in the case of small seed content so that a bimodal grain size distribution is apparent. As shown in Fig. 1 for Yb- and Y-SiAlONs at 0.5% seeding, Ca- and Nd-SiAlONs at 1% seeding, and Li-SiAlON at 6% seeding, a bimodal distribution has developed in each ceramic. The matrixes of fine grains are characteristic of the microstructures of unseeded ceramics prepared under similar firing conditions. Note that large grains in Ca1512 and Nd1312 are needlelike, large grains in Y1512 and Yb1512 are elongated but with a modest aspect ratio, and large grains in Li-1512 are equiaxed.

To quantify the above difference, we have analyzed the grain statistics to calculate the average aspect ratio of large grains in these bimodal distributions. To identify the grains that are most
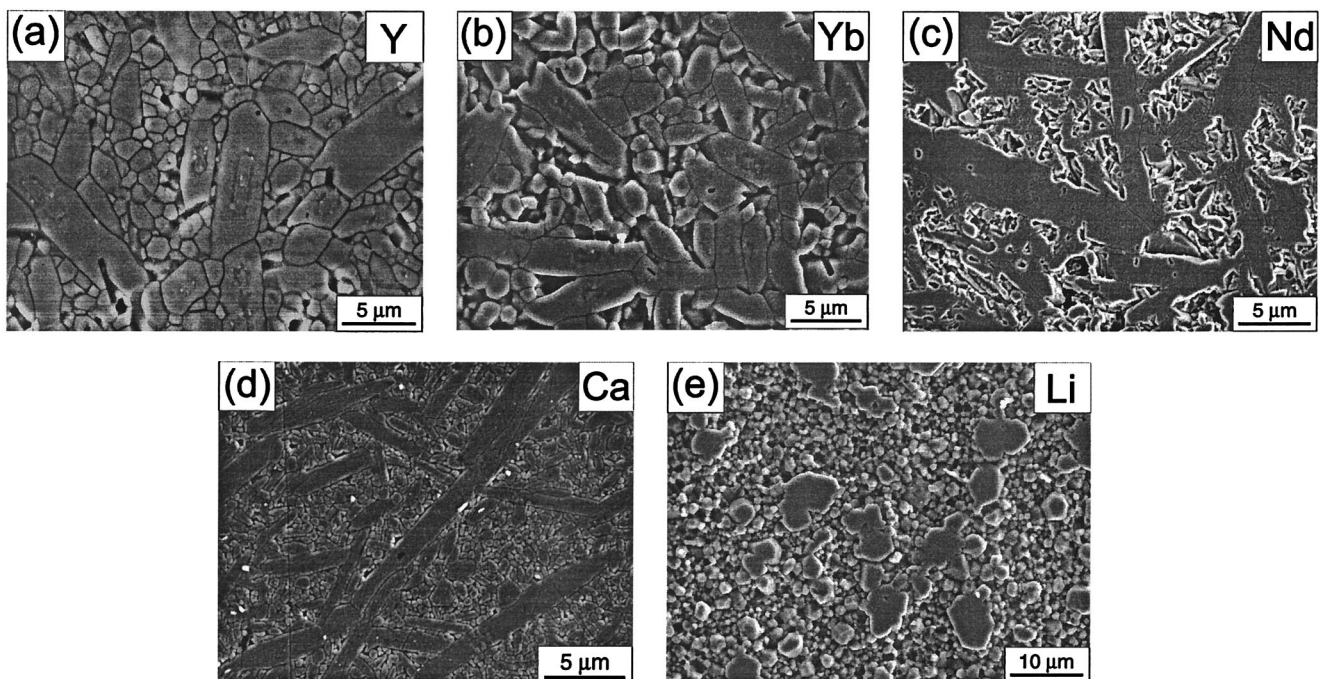
Fig. 1. Bimodal microstructure of (a) Y1512 with 0.5% seeds, (b) Yb1512 with 0.5% seeds, (c) Nd1311 with 1% seeds, (d) Ca1512 with 1% seeds, and (e) Li1512 with 6% seeds. Many grains in (a) and (b) have a core–shell appearance.

likely derived from the seeds, we first inspected the statistics of unseeded ceramics and determined the grain area of the 95th percentile. This established a threshold that was next used to filter the data of seeded ceramics; namely, the grains that are beyond the threshold are considered to have grown from seeds. Of the latter population, the aspect ratio at the 90–95th percentile was then determined. This aspect ratio is plotted in Fig. 2 against the radius of the cation (for 6-fold coordination.) A positive correlation is evident.

(2) Optimization and Saturation of Microstructure

From a practical point of view, the optimal microstructure that corresponds to the highest fracture toughness is of great interest. These optimized microstructures are shown in Fig. 3 for each SiAlON based on the highest R-curve/toughness data to be shown in Section III(4). The optimization occurs at different seeding levels, 1% for Y1512 and Yb1512, 5% for Nd1311, 4%–8% for Ca1512, and 12% for Li1512. Different grain shapes are also obvious in the optimized microstructure: the grains of Y1512 and Yb1512 have a lower aspect ratio than those of Ca1512 and Nd1311, while the grains of Li1512 are all equiaxed.

The microstructure of seeded ceramics may saturate as the concentration of seeds increases, at concentrations past the optimal ones for peak toughness. At 5% seeding, the microstructure of Y-SiAlON contains essentially equiaxed grains with a smaller size than that at lower seed concentrations (see Fig. 2(d) in Part I). The microstructure of Yb1512 at 5% seeding shows the same characteristics (micrograph not shown here). On the other hand, in Ca1512, there is no saturation even at 8% seeding when the microstructure still contains a high density of elongated grains (see Fig. 2(c) in Part II). This trend was also observed in Nd1311 when, at 7.5% seeding, many elongated grains were visible (micrograph not shown here). However, as also noted in Part II, blocky grains due to grain coalescence are quite common in the microstructure of Ca1512 at high seeding levels. The same is true with Nd1311. In contrast, large and mostly isolated equiaxed grains are observed in Li1512 even at 18% seeding. Therefore, no saturation is apparent in this ceramic.

(3) Seeding Statistics

Seed crystals were readily revealed in seeded Y1512 and Yb1512 using the etching method in our experiment. As shown in Figs. 1(a,b) and 3(a,b), some grains have a core–shell appearance with the cores obviously corresponding to the seeds. The statistics of these grains have been analyzed. Their area fraction (f_s^*), average width (W), and aspect ratio (AR), as well as their number per unit area (N_a^*), also called the area concentration, are listed in Table II. It is clear that as the amount of seeds increases, the width and the aspect ratio of grains decrease. It is also clear that while the area concentration of large grains gradually increases with the

amount of seeds, their area fraction is relatively constant. Indeed, the area concentration does not increase as fast as the amount of seeds does. These observations support the notion that there is competition in the grain growth from neighboring seeds and that the microstructure shows a trend toward saturation at high seeding levels.

To further analyze seeding statistics and to understand their relation to the control and saturation of the microstructure, we have adopted a model that assumes that both grains and seed crystals have the shape of a circular rod with a radius R ($R = W/2$) and R_s ($R_s = W_s/2$), respectively. We also assume that they are concentric. In hot-pressed SiAlONs, most elongated grains have a preference to lie close to the hot-pressing plane. We can then calculate the average cross section of an elongated grain on the polished section—for both those that reveal their seeds and those that do not. This statistical analysis is outlined in Appendix A. We can next compute the "true" area fraction (f_s) of seeded grains, including those that are seeded but do not reveal their seeds on the polished section. This value, which is also listed in Table II, is quite close to unity for most samples of Y1512 and Yb1512, indicating that essentially the entire ceramic is made of grains that grew from seed crystals.

We have also estimated the number of seeds (N_s), per unit area, that could cause a grain to grow so that both the seed and the grain are revealed on the (randomly chosen) polished cross section. This analysis is given in Appendix A, too. In addition, some grains that grew from seeds may also reach the polished cross section, but their seeds are not revealed because they lie entirely beneath the surface. Therefore, a statistical estimate of the "true" area concentration (N_a) of all grains that grew from seeds and reached the cross section, with or without having their seeds revealed, is also given in Appendix A. The estimated N_a and N_s are listed in Table II. These two numbers are relatively close to each other for seed amounts of 1% or less. At larger seed amounts the estimated number of seeds is definitely higher than the number of large grains observed. Therefore, not all seeds are independently operative at higher concentrations.

(4) Fracture Toughness and Grain Statistics

Rising R-curves of Y1512 and Ca1512 that are strongly influenced by seeding have been previously reported in our work[2–4] and are reproduced here in Fig. 4. R-curves have also been obtained for Nd1311 and Yb1512, as shown in Fig. 4. They follow similar behavior. In all cases, the R-curves in the seeded ceramics are higher than those of unseeded ceramics. Both the peak value and the slope of the curve increase when seeding approaches the optimal level, beyond which they begin to decrease. The fracture resistance, after 1000 μm of crack propagation, is plotted in Fig. 5(a) as a function of seed amount for each SiAlON. (Li-SiAlON has no R-curve behavior, so the data used are those of SENB fracture toughness.) This plot was used to identify the optimal microstructures shown in Fig. 3. The peak toughness is highest in Y1512 and lowest in Li1512.

To correlate the fracture resistance with the microstructure, we are guided by the model of grain pullout,[13–16] which envisions frictional work as the main source of fracture energy. A summary of the prediction of this model, which ignores the near-tip toughening mechanism (such as elastic bridging due to grain bending) and is thus most appropriate at very long crack propagation lengths, is given in Appendix B. If grains are short enough to be completely pulled out in the wake of a crack tip, the model[15,16] predicts that the frictional work of the ith grain is proportional to the volume fraction (V_i), the grain width (W_i), and the (aspect ratio)^2 or (AR$_i$)^2 of such grain. It follows that the quantity

$$I = C \sqrt{\sum_i (V_i W_i)(\mathrm{AR}_i)^2} \qquad (1)$$

which may be evaluated using the statistical data for all grains in each microstructure, is an indicator of fracture toughness. Here, C is a constant that may be used as a fitting parameter, which in turn
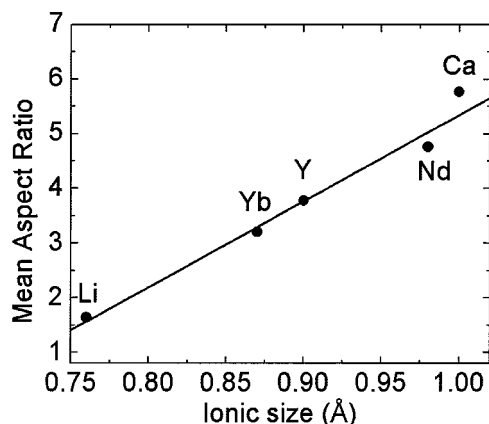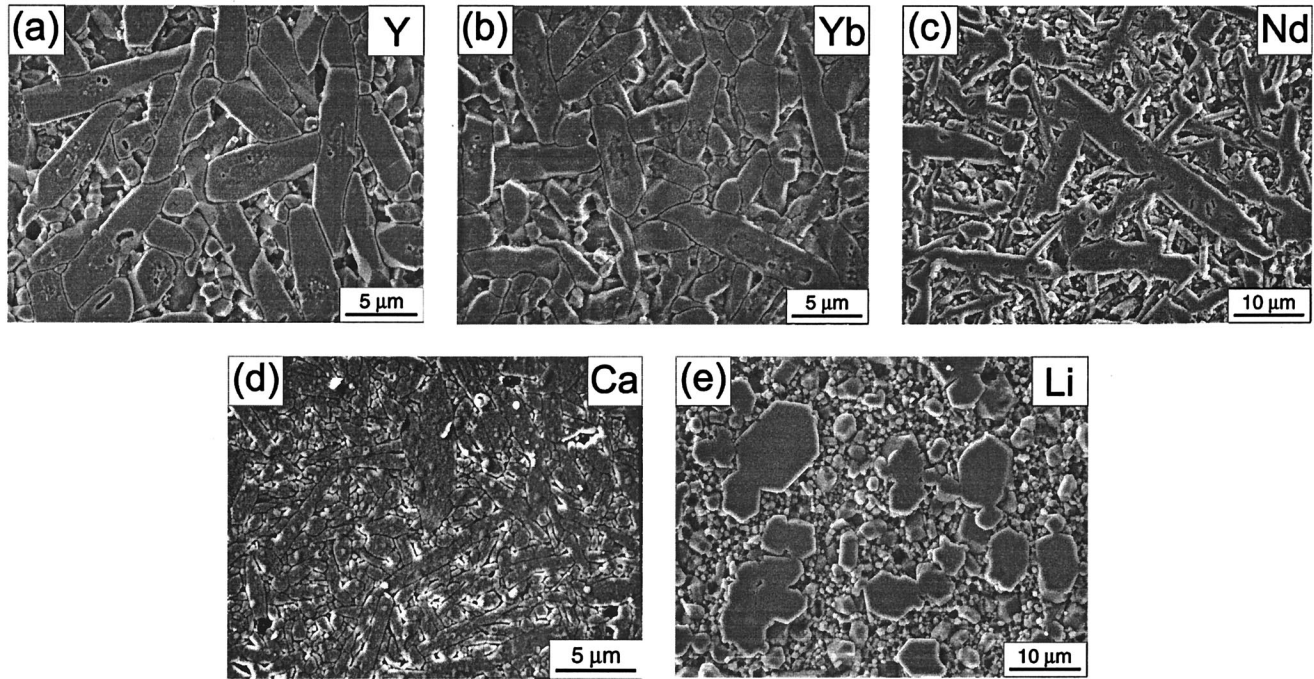

Fig. 2. Correlation between aspect ratio of large grains (see text) in Fig. 1 and ionic radius of interstitial cations (6-fold coordination.)

Fig. 3. Nearly optimized microstructure of (a) Y1512 with 1% seeds, (b) Yb1512 with 1% seeds, (c) Nd1311 with 5% seeds, (d) Ca1512 with 4% seeds, and (e) Li1512 with 12% seeds.

can be compared with Eq. (A-3) in Appendix A. This indicator is shown in Fig. 5(b) using the same C for all SiAlONs. We see that the calculated I closely follows the trend of the fracture toughness of Y1512 and Yb1512, in that a maximum is located at 1% seeding, and likewise for Nd1512 for which a maximum is located at 5%, Ca1512 with a maximum at 4%–8% as seen in the toughness data, and Li with a maximum at >12%. Referring to I in Eq. (1) again, we further find that it would indicate the toughness to rank in the order of Y > Yb > Nd > Ca > Li. This is essentially correct considering the fracture toughness data of different ceramics. Indeed, by letting $C = 2.4$ MPa·m$^{1/2}$/μm$^{1/2}$, the entire fracture toughness data of all of the samples can be reproduced using I following Eq. (1).

IV. Discussion

(1) Ionic Size Effect

The positive correlation between the aspect ratio of seeded grains and the radius of modifying cations is central to the development of different microstructures of α-SiAlONs. This correlation is also seen in the shapes of seed crystals. Comparing the length and width of seeds in Table I, we find increasing aspect ratio in the order of Li < Yb < Y < Ca < Nd, which is nearly identical to the one in Fig. 2. Note that the seed crystals were obtained using different firing conditions and liquid compositions. Therefore, a rigorous comparison of their morphology is difficult. Nevertheless, using a larger set of morphology data of seed crystals prepared in different liquids and under different firing conditions, we have been able to establish a similar correlation supporting the important role of cation radius in determining the aspect ratio.[6] These observations cannot be attributed to the stability and internal crystal structure of α-SiAlON. This is because, while Nd- and Ca-SiAlONs have similar aspect ratios, Nd-α-SiAlON is the least stable system among rare-earth-containing α-SiAlONs while Ca-α-SiAlON is very stable. Concerning crystal structure, the lattice parameters of α-SiAlON are known to be remarkably independent of the type of the interstitial cation that it contains, especially in the series of rare-earth-α-SiAlONs. Therefore, the internal crystal structure is probably irrelevant to the observed trend of grain shape or crystal shape.

Previously, Hoffmann reported that the aspect ratios of β-Si$_3$N$_4$ crystals grown from rare-earth-Al-Si-O-N glasses increased with the ionic radii of rare earths (including Y).[17] We now believe that, for α-SiAlONs, the same holds for cations from other groups in the

Table II. Area Fraction (f_s^*), Average Width (W), Aspect Ratio (AR), and Area Concentration (N_a^*) of Grains with a Core–Shell Appearance, at Different Seed Contents (F_s)[†]

F_s (%)	f_s^* (%)	W (μm)	AR	N_a^* (μm^{-2})	f_s (%)	N_a (μm^{-2})	N_s (μm^{-2})
			Yttrium				
0.5	30.7	2.76	3.65	0.010	93.7	0.049	0.048
1	31.4	2.63	2.79	0.015	91.4	0.060	0.074
2.5	42.7	2.46	2.24	0.029	116.2	0.096	0.148
5	48.8	2.26	1.91	0.045	122.0	0.128	0.244
			Ytterbium				
0.5	34.6	2.52	2.59	0.019	112.3	0.087	0.060
1	39.3	2.23	2.60	0.029	112.8	0.118	0.107
2.5	36.3	1.58	2.25	0.055	73.8	0.147	0.171
5	35.6	1.51	1.89	0.075	69.2	0.175	0.291

[†]Also listed are the estimated actual area fraction (f_s), actual concentration of seeded grains (N_a), and concentration of seeds per area (N_s) from which grains may grow to reach a polished section. (See text.)
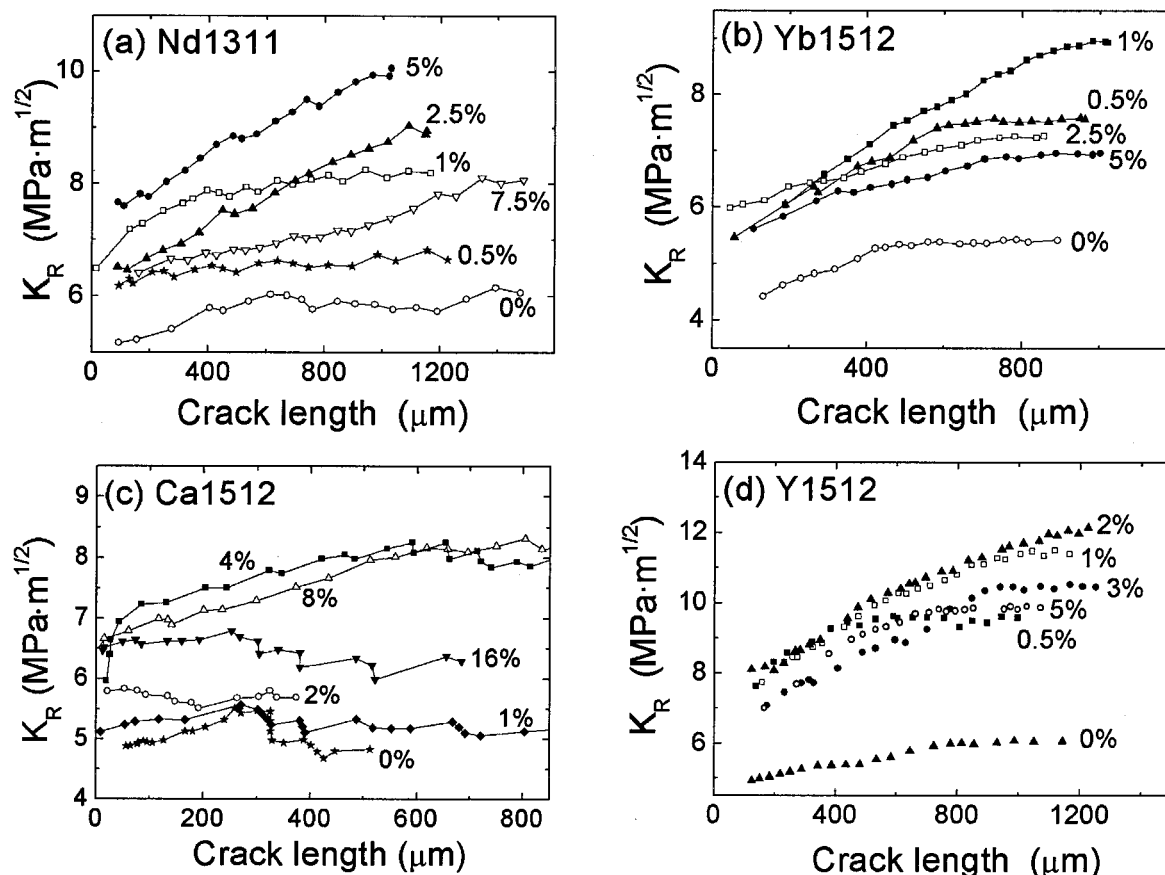
Fig. 4. *R*-curves of (a) Nd1311, (b) Yb1512, (c) Ca1512, (d) Y1512 at different seeding levels shown in percentage.

periodic table, and for both ceramics and liquid-grown crystals. It would seem plausible that the size effect operates through the segregation of larger cations to the prismatic interface of the crystal or grain, retarding growth kinetics. Direct evidence of such interface segregation, however, is still lacking and would be desirable for a better understanding of the origin of the ionic size effect.

(2) Effect of Aspect Ratio

The aspect ratio has important effects on other metrics of microstructure as well. Assuming the same seeding efficiency and the same overall volumetric growth of seeded grains, we expect a smaller grain width to accompany a higher aspect ratio. This effect is indeed observed. For example, the grain width in Fig. 1 increases in the order of Ca < Nd < Y = Yb < Li. Grains of higher aspect ratio also experience earlier impingement at a point when the concentration and the volume fraction of elongated grains are still low. (As the aspect ratio increases toward infinity, the impingement concentration and volume fraction both approach zero.) This would leave a microstructure featuring many regions that are sparsely populated by needlelike grains. In such a case, to reach optimal toughness, more seeds need to be added to fill the remaining space with elongated grains. This different behavior is illustrated in Fig. 6 using simulated two-dimensional microstruc-
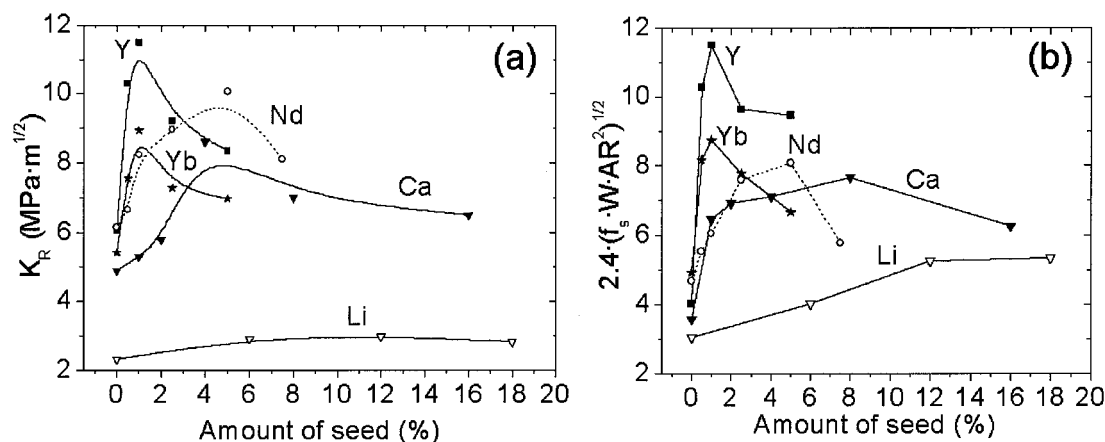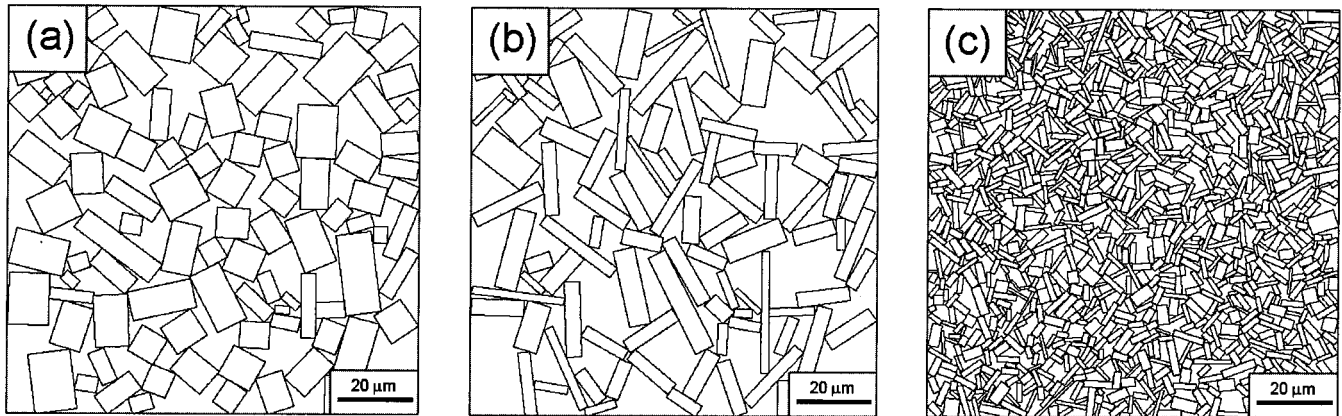

Fig. 5. (a) K_R versus seed percentage for various α-SiAlONs. The data of Li1512 are SENB toughness. (b) Predicted fracture toughness (in MPa·m$^{1/2}$) using the measured grain fraction, grain width, and aspect ratio, with $C = 2.4$ MPa·m$^{1/2}$/μm$^{1/2}$.

Fig. 6. Computer-simulated two-dimensional microstructures with various growth anisotropy and seed amounts. Growth anisotropy is defined by the ratio of length to the width growth rate, V_L/V_W. Growth proceeds until impingement in either the length or the width direction occurs; after that rearrangement by translation is allowed and growth continues until the final impingement in both the length and the width directions. Initial sizes of seeds in all cases follow a normal distribution with length $L = 1.71 \pm 0.63$ μm and width $W = 0.71 \pm 0.193$ μm. The final area fraction of grains A is also indicated: (a) 1% seed, $V_L/V_W = 1$, $A = 62\%$; (b) 1% seed, $V_L/V_W = 5$, $A = 48\%$; (c) 10% seed, $V_L/V_W = 5$, $A = 58\%$. Further details of the simulation will be reported elsewhere.

tures containing elongated grains of different aspect ratios. (See the caption of Fig. 6 for more details.) As shown in Figs. 6(a) and (b), the area fraction of elongrated grains at impingement decreases from 62% (Fig. 6(a)) to 48% (Fig. 6(b)), at 1% seeding, as the aspect ratio increases. In the case of the larger aspect ratio, the area fraction of elongated grains can reach only 58% (Fig. 6(c)) even at 10% seeding. This qualitatively explains why the optimum seeding level is 1% in Yb1512 and Y1512, which have similarly modest aspect ratios, but 5% in Nd1311 and 4%–8% in Ca1512, which have similarly high aspect ratios.

Of course, the volumetric growth rate of seeded grains, as well as seeding efficiency, is somewhat different in different systems. For example, Y1512 and Yb1512 have high seeding efficiency at least up to 1% seeding, and it was also concluded in Part II that Ca1512 has a high seeding efficiency at least up to 2%. On the other hand, it seems that Li1512 has very low seeding efficiency, since at 1% or 2% seeding very few large grains could be observed. This might be related to the apparent lack of anisotropy in grain growth in Li1512, which may imply that there is little energetic or kinetic advantage for the seeded grains compared with the matrix, consisting of unseeded grains.

(3)   *Grain Pullout in α-SiAlON*

The encouraging correlation between the microstructure parameters embodied in Eq. (1) and the fracture toughness of α-SiAlONs studied here strongly supports the model of grain pullout. In particular, the fact that a common fitting parameter, *C*, can provide a good correlation for all of the systems suggests that those nongeometrical parameters in the model, namely intergranular friction τ and the probability of grain boundary decohesion, are relatively insensitive to the composition. The fitting parameter *C* can be directly compared with the prediction of Appendix A to give an estimated τ of 108 MPa ($C = 2.4$ MPa·m$^{1/2}$/μm$^{1/2}$ and using $\nu = 0.24$, $E = 300$ GPa for α-SiAlON), which is of a reasonable magnitude. Of course, it should be cautioned here that the τ estimated above may not be the actual interfacial friction. This is because decohesion probability was not considered in our model, neither was the possibility of grain pullout at an inclined angle.

While the assumption of grain pullout as the main mechanism responsible for the observed toughening effect is probably correct for the SiAlON ceramics after a long crack extension, the steep rise of the *R*-curves in some cases after rather short crack extension suggests that the near-tip (elastic) bridging phenomena may also be present sometimes. The latter effect could also be hidden in the "apparent" crack-initiation toughness values, which may be defined by the extrapolation of the *R*-curves to zero crack extension and seem to be different in

different materials. This aspect was not investigated in our work, but may warrant further study to understand the crack-tip phenomena in different SiAlON systems.

V.   Conclusions

(1)   The microstructure and fracture behavior of seeded α-SiAlON strongly depend on the ionic radii of modifying cations. Moreover, since there is a one-to-one correspondence between large, reinforcing grains and seed crystals, at least at low seeding levels, the SiAlON microstructure can be accurately controlled by judicious seeding.

(2)   A larger ion causes an increase in the aspect ratios of grains. The highest aspect ratio is observed in Ca- and Nd-containing α-SiAlONs while a medium aspect ratio was observed in Y- and Yb-containing α-SiAlONs. Li-SiAlON has only equiaxed grains.

(3)   Grain impingement occurs earlier in microstructures with more elongated grains, at a relatively low volume fraction of such grains. To reach an optimal toughness, a higher seeding amount is needed. The optimal toughness of Ca- and Nd-SiAlONs requires 4%–8% seeding while only 1% seeding provides maximal toughening in Y- and Yb-SiAlONs.

Appendix A

Two Concentric Cylinders and Their Random Cross Sections

To model a grain with a seed, we consider two concentric cylinders of radii R and R_s and of lengths L and L_s, for the grain and the seed, respectively. Obviously, $R > R_s$ and $L > L_s$; in most cases, we also have $L > R$ and $L_s > R_s$. The polished cross section can be regarded as a random cross section of the grain, which may or may not intersect the seed. The grains that have a core–shell microstructure correspond to the ones for which the cuts intersect the seeds. The statistics of such grains are directly measurable. Our task is to estimate the statistics of all the grains that grow from seeds whether they reveal a core–shell microstructure or not. We do so by comparing the statistics of those cuts that intersects the seeds and those that do not.

If grains are parallel to the hot-pressing plane, which coincides with the polished section, then a random cut of the cylinder in the

axial direction has a probability R_s/R of intersecting the seed. If it does, then the average intersect cross section of the grain is

$$A* = L\left[\frac{1}{R_s}\int_0^{R_s} 2\sqrt{R^2 - \Delta^2}\, d\Delta\right] \quad (A-1)$$

where the bracketed expression on the right-hand side is the average length of the arc intersecting the seed. After integration, we obtain

$$A* = RL[\sqrt{1 - (R_s/R)^2} + (R/R_s)\sin^{-1}(R_s/R)] \quad (A-2)$$

that is $\sim 2RL$ for $R_s < R/2$. More generally, a random cut, whether it intersects the seed or not, has an average cross section A that is obtained by setting $R_s = R$ in Eq (A-2), $A = \pi RL/2$. The latter event has the probability of unity. Therefore, the ratio of the actual area fraction (f_s) of grains that are derived from seeds to the observed area fraction (f_s^*) of grains that have a core–shell appearance is

$$f_s/f_s^* = (R/R_s)(A/A*) \quad (A-3)$$

For $R_s < R/2$, the following approximate result holds:

$$f_s = (\pi R/4R_s)f_s^* = (\pi W/4W_s)f_s^* \quad (A-4)$$

The last equality above was obtained by substituting radius by one-half of the width, which is measurable.

Next we relate the number of core–shell grains per unit area (N_a^*) to the number of seed-containing grains per unit area (N_a). If the grain again lies on the hot-pressing plane which coincides with the polished cross section, then the probability that the seed is cut is again R_s/R. So the ratio of N_a to N_a^* is simply R/R_s, i.e.,

$$N_a = (R/R_s)N_a^* = (W/W_s)N_a^* \quad (A-5)$$

Lastly, we estimate the number of seeds (N_s), per unit area, that could cause a grain to grow and reach a random cross section. If we also assume the grain to lie on the hot-pressing plane, then the center axis of the seed must lie within a distance R from the random cross section to allow the grain to intersect the cross section. For each unit area of the cross section, therefore, there is a zone of a height $2R$ within which the seed may lie. (The factor 2 enters because the seed may be on either side of the cross section.) To estimate N_s, we multiply this volume by the volume fraction of seeds (F_s, obtained from percent of seeding), and divide the product by the volume per seed ($\pi L_s R_s^2$). This gives

$$N_s = 2RF_s/\pi L_s R_s^2 = 4WF_s/\pi L_s W_s^2 \quad (A-6)$$

The above quantity may be compared with N_a to assess the efficiency of seeding.

In reality, we have also seen grains that grow at an inclined angle to the hot-pressing plane. This inclination has the largest effect on N_s, since it allows grains that originate from those seeds as far as $L/2$ away to reach the cross section. Assuming, in the extreme, all grains are normal to the hot-pressing plane, we arrive at a new estimate of N_s which is

$$N_s = 4LF_s/\pi L_s W_s^2 \quad (A-7)$$

For self-consistency, we also arrive at a new estimate of N_a

$$N_a = (L/L_s)N_a^* \quad (A-8)$$

In this work, we have evaluated f_s using Eq. (A-4), N_a using the average values of Eqs. (A-5) and (A-8), and N_s using the average values of Eqs. (A-6) and (A-7). These estimated values, along with the measured values of f_s^* and N_a^*, are listed in Table II.

Appendix B

Fracture Toughness Due to Grain Pullout

We summarize the basic results of the toughening model due to grain pullout,[13–16] which envisions frictional work as the main source of fracture energy. The basic assumption is that, before pullout, decohesion of a grain has taken place along the grain boundary and possibly by intergranular fracture, so the only resistance to pullout is from intergrain friction on the side surfaces. Let the length and the radius of this "free" grain be l and R, respectively, and assume that it is normal to the crack surface. Then the stress–displacement (σ–u) relationship during pullout is given by

$$\sigma(l,u) = 2\tau(l - u)/R = 4\tau(l - u)/W = 4\tau(l - u)/W \quad (B-1)$$

In the above, τ is the interfacial friction, and $W = 2R$ is grain width.

We assume grains are short enough so that debonding always extends to the full length of the grain. Since the crack may intercept a grain at any height, pullout may take place with a "free" grain length varying from 0 to $L/2$, where L is the grain length. So the average frictional work of pulling out such grains is obtained by the following integral:[15]

$$G = V\int_0^{1/2}\frac{dx}{L/2}\int_0^x \sigma(x,u)\, du = \left(\frac{1}{6}\right)V_\tau W(AR)^2 \quad (B-2)$$

In the above, V is the volume fraction of such grains, and the aspect ratio AR is L/W. The fracture toughness can then be calculated from the following equality:

$$K = \sqrt{\frac{EG}{1 - \nu^2}} = \sqrt{\frac{E\tau}{6(1 - \nu^2)}}\sqrt{VW(AR)^2}$$
$$= C\sqrt{VW(AR)^2} \quad (B-3)$$

Here E is Young's modulus and ν is Poisson's ratio, under the plane-strain condition; and C is a corresponding constant. The above results can be readily generalized to include a spectrum of grains of different length and radius, as expressed by Eq. (1) in the text.

References

[1]J. Kim, A. Rosenflanz, and I-W. Chen, "Microstructure Control of *In Situ* Toughened α′-SiAlON Ceramics," *J. Am. Ceram. Soc.*, **83** [7] 1819–21 (2000).

[2]M. Zenotchkine, R. Shuba, J.-S. Kim, and I-W. Chen, "R-Curve Behavior of *In Situ* Toughened α-SiAlON Ceramics," *J. Am. Ceram. Soc.*, **84** [4] 884–26 (2001).

[3]M. Zenotchkine, R. Shuba, and I-W. Chen, "Effect of Seeding on the Microstructure and Mechanical Properties of α-SiAlON: I, Y-SiAlON," *J. Am. Ceram. Soc.*, **85** [5] 1254–59 (2002).

[4]R. Shuba and I-W. Chen, "Effect of Seeding on the Microstructure and Mechanical Properties of α-SiAlON: II, Ca-SiAlON," *J. Am. Ceram. Soc.*, **85** [5] 1260–67 (2001).

[5]M. Zenotchkine, R. Shuba, J.-S. Kim, and I-W. Chen, "Synthesis of α-SiAlON Seed Crystals," *J. Am. Ceram. Soc.*, **84** [7] 1651–53 (2001).

[6]M. Zenotchkine, R. Shuba, and I-W. Chen, "Liquid Phase Growth of Small Crystals for Seeding α-SiAlON Ceramics," submitted to *J. Am. Ceram. Soc.*

[7]M. Zenotchkine, R. Shuba, and I-W. Chen, "Effect of Heating Schedule on the Microstructure and Fracture Toughness of α-SiAlON—Cause and Solution," *J. Am. Ceram. Soc.*, **85** [7] 1882–84 (2002).

[8]Z.-K. Huang and D.-S. Yan, "Phase Relationships in Si_3N_4–AlN–M_XO_Y System and Their Implications for Sialon Fabrication," *J. Mater. Sci.*, **27**, 5640–44 (1992).

[9]W.-Y. Sun, T.-Y. Tien, and T.-S. Yen, "Solubility Limits of α-SiAlON Solid Solutions in the System Si,Al,Y/N,O," *J. Am. Ceram. Soc.*, **74** [10] 2547–50 (1991).

[10]J. W. T. van Rutten, H. T. Hitzen, and R. Metselaar, "Phase Formation of Ca α-SiAlON by Reaction Sintering," *J. Eur. Ceram. Soc.*, **16**, 995–99 (1996).

[11]Z. B. Yu, D. P. Thompson, and A. R. Bhatti, "Preparation of Single Phase Lithium α-Sialon," *Br. Ceram. Trans.*, **97** [2] 41–47 (1998).

[12]A. I. Mamchik, J. S. Kim, and I-W. Chen, "A New Method for Etching Silicon Nitride Ceramics"; p. 191 in Abstracts of the 101st Annual Meeting and Exposition of the American Ceramic Society. American Ceramic Society, Westerville, OH, 1999.

[13]P. F. Becher, H. T. Lin, S. L. Hwang, M. J. Hoffmann, and I-W. Chen, "The Influence of Microstructure on the Mechanical Behavoir of Silicon Nitride Ceramics," *Mater. Res. Soc. Symp. Proc.*, **287**, 147–58 (1993).

[14]P. F. Becher, S. L. Hwang, H. T. Lin, and T. N. Tiegs, "Microstructural Contribution to the Fracture Resistance of Silicon Nitride Ceramics"; pp. 87–100 in *Tailoring of Mechanical Properties of Si₃N₄ Ceramics*. Edited by M. J. Hoffmann and G. Petzov. Kluwer Academic Publishers, Dordrecht, Netherlands, 1994.

[15]I-W. Chen, S.-Y. Liu, and D. Jacobs, "Effect of Temperature, Rate and Cyclic Loading on the Strength and Toughness of Monolithic Ceramics," *Acta Metall. Mater.*, **43** [4] 1439–46 (1995).

[16]S.-Y. Liu and I-W. Chen, "High Temperature Crack Growth in Silicon Nitride under Static and Cyclic Loading: Short-Crack Behavior and Brittle–Ductile Transition," *Acta Metall. Mater.*, **44** [5] 2079–92 (1996).

[17]M. J. Hoffmann, H. Gu, and R. M. Cannon, "Influence of the Interfacial Properties on the Microstructural Development and Properties of Silicon Nitride Ceramics," *Mater. Res. Soc. Symp. Proc.*, **586**, 65–74 (2000).   □